Journal of *Marine Science and Engineering*

MDPI

Article

Underwater Tone Detection with Robust Coherently-Averaged Power Processor

Qichen Xie [1,2,3], Cheng Chi [1,2,*], Shenglong Jin [1,2], Guanqun Wang [1,2], Yu Li [1,2] and Haining Huang [1,2]

[1] Institute of Acoustics, Chinese Academy of Sciences, Beijing 100190, China
[2] Key Laboratory of Science and Technology on Advanced Underwater Acoustic Signal Processing, Chinese Academy of Sciences, Beijing 100190, China
[3] University of Chinese Academy of Sciences, Beijing 100049, China
* Correspondence: chicheng@mail.ioa.ac.cn

Abstract: The detection of tonal signals with unknown frequencies is an important area of study in underwater signal processing. A common approach to address this issue is to use the Discrete Fourier Transform (DFT) for observations. When a tone does not lie precisely at the discrete DFT frequency point, its energy will leak to adjacent frequency point. This phenomenon is known as scalloping loss or Picket Fence Effect (PFE). PFE leads to the degradation of detection performance based on DFT. This paper studies the problem of robust detection in the case of PFE. A coherently-averaged power processor utilizing the information of adjacent frequency bins is designed. The results of simulations and experiments show that the proposed method is robust against PFE, and is highly suitable for tone detection in practical circumstances.

Keywords: tone detection; phase compensation; coherent averaging; picket fence effect; passive sonar

Citation: Xie, Q.; Chi, C.; Jin, S.; Wang, G.; Li, Y.; Huang, H. Underwater Tone Detection with Robust Coherently-Averaged Power Processor. *J. Mar. Sci. Eng.* **2022**, *10*, 1505. https://doi.org/10.3390/jmse10101505

Academic Editors: Jacopo Aguzzi, Giacomo Picardi, Damianos Chatzievangelou, Simone Marini, Sascha Flögel, Sergio Stefanni, Peter Weiss and Daniel Mihai Toma

Received: 10 September 2022
Accepted: 12 October 2022
Published: 16 October 2022

1. Introduction

Over the past several decades, the detection of tonal (sinusoidal) signals embedded in noise has continuously received attention in many fields, such as sonar, radar, communication, seismology, and ocean engineering. Noise radiated from vessels consists of a mixture of broadband noise and tonal noise, mainly caused by mechanical vibration and propeller propulsion [1]. The tonal component contains the characteristics of the ship and is of great importance for target detection and recognition [2]. And marine experiments have proved that low-frequency tonal signals can propagate over a long distance and maintain remarkable phase stability [3]. Therefore, tone detection has received considerable attention in acoustic signal processing.

The problem of detecting tonal signals with unknown parameters is usually expressed as a problem of composite hypothesis testing [4,5]. There are several solutions to this problem by utilizing the statistical characteristics of DFT in different segments. A common and extensively used method is to reduce the variability in signals and noise and increase the Signal-to-Noise Ratio (SNR) by averaging process, which is referred to as the Average Power Processor (AVGPR) [6,7]. Another widely-used method is the Generalized Likelihood Ratio Test (GLRT) [8] for composite hypothesis test, which performance close to the optimal bound, especially under low probability of false alarm [9,10]. However, only the amplitude information of the tonal signals is used in these two methods. Consequently, the detection performance tends to decay due to the loss of phase information. In order to take full advantage of the phase information, a phase estimation method has been proposed and the performance of the GLRT has been greatly improved by compensating the phase difference among segments, which is referred to as the Coherent Generalized Likelihood Ratio Test (CGLRT) [11]. The AVGPR can also be enhanced by introducing phase compensation to coherently average segments, and is named as the Coherently-Averaged Power Spectral Estimate (CAPSE) [12].

However, the ship radiated noise is also gradually reduced with the development of propeller control and mechanical noise suppression technology [13,14]. Therefore, the aforementioned detectors need to be further improved, which is also the purpose of this study. Theoretically, if the tonal signal is stable enough within the observation time, the processing gain of DFT increases with the increase of DFT points [15]. However, the tonal signal usually jitters or drifts in the actual situation because of the change in machine working conditions [16], mechanical fault [17], Doppler effect [18], and so on. Therefore, the length of DFT is limited in order to increase the robustness to signal instability. Due to the discrete nature of Discrete Fourier Transform (DFT), when a tone does not align with the center of the DFT frequency bin or lie precisely on the discrete DFT frequency point, then the signal energy will leak to the adjacent frequency point. It will degrade the performances of the above detectors and is known as scalloping loss or Picket Fence Effect (PFE) [19]. PFE deserves special attention in DFT-based detectors because their performance can be improved by solving it.

In the present study, a frequency bin joint coherent AVGPR that is robust to the performance degradation caused by PFE is developed. It utilizes the information of adjacent DFT frequency bins to gather the leaked energy of signal. Simulation is carried out to analysis the performance of the detectors in the presence and absence of the PFE. A sea experiment is conducted to compare the reliability of the methods.

The remainder of this paper is organized as follows: Section 2 describes the models and presents the detection problem. Next, the proposed detector is detailed in Section 3. Simulations are presented in Section 4, for the purpose of comparing the performances of the examined detectors. The experimental results are detailed in Section 5. Finally, the conclusions reached in this study are given in Section 6.

2. Problem Statement

2.1. Model

In general, the detection problem can be considered as a choice between two hypotheses H_0 and H_1, where H_0 represents only noise and H_1 represents the presence of signal. This can be expressed as [4]:

$$\begin{aligned} H_0 &: x(n) = g(n) \\ H_1 &: x(n) = s(n) + g(n) \end{aligned} \tag{1}$$

where $x(n)$ is observation; $s(n) = A\exp[j(\omega_0 n + \varphi)]$ is the tonal signal to be detected with unknown amplitude A, unknown initial phase φ and unknown normalized angular frequency ω_0, $\omega_0 = 2\pi f_0/f_s$; f_0 is the tone frequency; f_s is the sampling rate; and $g(n)$ is an additive White Gaussian Noise (WGN) with zero mean and unknown variance σ_g^2.

In order to increase the robustness to signal instability while taking advantage of the DFT processing gain, it is usually used to segment the observation, take the DFT of the segments, and average the DFT results [6]. In this study, the observation sequence $x(n)$ is divided into L segments of length N with sliding length M as follows:

$$\begin{aligned} x_l(n) &= x(l \cdot M + n) \\ &= A\exp[j(\omega_0 n + \omega_0 lM + \varphi)] + g_l(n) \\ &n = 0, \ldots, N-1;\ l = 0, \ldots, L-1. \end{aligned} \tag{2}$$

Figure 1a illustrates the segmentation of observation sequence. The segments can be overlapped if $M < N$ and contiguous if $M = N$. Assume that the total number of observation data $x(n)$ is L_x. The relationship among L, N, M and L_x is shown as follows, where $\lfloor \cdot \rfloor$ is the rounding down notation:

$$L = \left\lfloor \frac{L_x - N}{M} \right\rfloor + 1. \tag{3}$$

The DFT of a segment can only observe the spectrum on a limited number of N frequency points. When the signal frequency is aligned with the center of a DFT frequency bin or at the discrete DFT point, the full amplitude in that bin is obtained. Otherwise, when the signal frequency is between two discrete DFT frequency points (such as $k-1$ and k in Figure 1b), the energy of the signal leaks to the adjacent frequency bins, causing a reduced amplitude split between the two bins, as illustrated in Figure 1b, where the digital frequency of the ω_0 is k_0^*, $\omega_0 = \frac{2\pi k_0^*}{N}$ for N-point DFT, $k_0^* = k_0 + \Delta$, k_0 is the integer closest to k_0^* and $|\Delta| \leq 1/2$. The N-point DFT of $x_l(n)$ is expressed as follows:

$$\begin{aligned} X_l(k) &= \sum_{n=0}^{N-1} x_l(n) \exp\left(-j\tfrac{2\pi kn}{N}\right) \\ &= S_l(k) + G_l(k) \\ &k = 0, \ldots, N-1 \end{aligned} \tag{4}$$

where

$$\begin{aligned} S_l(k) &= \sum_{n=0}^{N-1} s_l(n) \exp\left(-j\tfrac{2\pi kn}{N}\right) \\ &= A \exp\left[j\left(\tfrac{2\pi Mk_0^*}{N} l + \varphi\right)\right] \sum_{n=0}^{N-1} \exp\left(-j2\pi \tfrac{k_0^* - k}{N} n\right) \\ &= A \tfrac{\sin\left[\pi\left(k_0^* - k\right)\right]}{\sin\left[\pi\left(k_0^* - k\right)/N\right]} \exp\left[j\left(\tfrac{2\pi Mk_0^*}{N} l + \varphi\right)\right] \exp\left[j\pi(k_0^* - k)\tfrac{N-1}{N}\right], \end{aligned} \tag{5}$$

$$G_l(k) = \sum_{n=0}^{N-1} g_l(n) \exp\left(-j\frac{2\pi kn}{N}\right). \tag{6}$$

A variant of Dirichlet kernel is used in the derivation of $S_l(k)$. $G_l(k)$ also has a complex Gaussian distribution with $G_l(k) \sim CN\left(0, N\sigma_g^2\right)$, since it is the linear combination of $g_l(n)$. When $k = k_0$, then $S_l(k_0)$ is obtained as follows:

$$S_l(k_0) = A \frac{\sin(\pi\Delta)}{\sin(\pi\Delta/N)} \exp\left[j\left(\frac{2\pi Mk_0^*}{N} l + \varphi\right)\right] \exp\left(j\pi\Delta\frac{N-1}{N}\right). \tag{7}$$

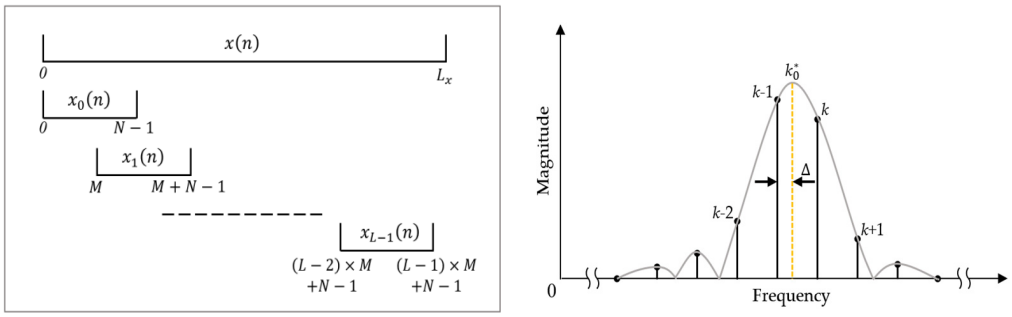

(**a**) (**b**)

Figure 1. Illustration of the model: (**a**) Segmentation of observe sequence. (**b**) Relationship among k, k_0, k_0^* and Δ; $k_0 = k-1$ when k_0^* is closer to $k-1$ and $k_0 = k+1$ when k_0^* is closer to $k+1$. .

2.2. Existing Detectors and Problem

The AVGPR [7] is a conventional averaging processor. It generally stabilizes signals more than the noise as the number of averaged segments increases, because the signals are usually more coherent than the noise. However, its shortcoming is that it only utilizes the amplitude information of the DFT. It can be expressed as follows:

$$T_{AVGPR} = \frac{1}{L} \sum_{l=0}^{L-1} |X_l|^2. \tag{8}$$

In order to use the phase information to achieve more processing gain, the phase difference $\exp\left(j\frac{2\pi Mk_0^*}{N}l\right)$ between $X_0(k)$ and $X_l(k)$ $(l = 0, \ldots, L-1)$ must be eliminated. This can be estimated by the R-point DFT (padding zeros if necessary) of the complex sequence $X_l(k)$, as follows:

$$W_k(v) = \sum_{l=0}^{R} X_l(k) \exp\left(-j\frac{2\pi vl}{R}\right),\ v = 0, \ldots, R-1. \tag{9}$$

The estimated phase difference $\delta(k)$ can be calculated by the following:

$$\delta(k) = \frac{\text{argmax}|W_k(v)|}{R}. \tag{10}$$

When $k = k_0$, then $\delta(k_0) = \frac{k_0^* M}{R}$. Multiplying $X_l(k)$ by $\exp[-j2\pi\delta(k)l]$ to compensate the phase difference, the coherent sequence $Y_l(k)$ is obtained as follows:

$$Y_l(k) = X_l(k) \exp[-j2\pi\delta(k)l]. \tag{11}$$

The CAPSE [12] can be considered as the windowed coherent AVGPR that utilizes phase information, and can be expressed as follows:

$$T_{CAPSE} = \frac{1}{L}\left|\sum_{l=0}^{L-1} Y_l\right|^2. \tag{12}$$

The GLRT replaces the unknown parameters by their Maximum Likelihood Estimations (MLEs). Although there the GLRT is not optimal, in practice, it appears to work quite well [4]. The CGLRT [11] is a combination of phase compensation and the GLRT, and is given by the following:

$$T_{CGLRT} = -L \ln \frac{\hat{v}_1}{\hat{v}_0}, \tag{13}$$

$$\hat{u} = \frac{1}{L}\sum_{l=0}^{L-1} Y_l(k), \tag{14}$$

$$\hat{v}_0 = \frac{1}{L}\sum_{l=0}^{L-1} |Y_l(k)|^2, \tag{15}$$

$$\hat{v}_1 = \frac{1}{L}\sum_{l=0}^{L-1} |Y_l(k) - \hat{u}|^2. \tag{16}$$

It is worth noting that the test statistics of AVGPR, CAPSE and CGLRT are all constructed with a single frequency bin sequence $X_l(k)$. When $\Delta \neq 0$, then the signal amplitude of $S_l(k_0)$ in Equation (7) attenuates from AN to $A\frac{\sin(\pi\Delta)}{\sin(\pi\Delta/N)}$, which is caused by PFE. The attenuated amplitude can cause a loss of processing gain up to 3.9 dB when $|\Delta| = 0.5$ and $N \geq 10$ [20]. Therefore, a tonal detector that is robust against PFE is of great importance in practice, particularly in low SNR circumstances.

3. Proposed Method

This section presents a Frequency bin Joint Coherently-Averaged Power Processor (denoted as FJ_CAVGPR) by jointly utilizing the information of adjacent DFT frequency bins. As shown in Figure 1b, when $\Delta \neq 0$, then the energy of k_0^* will leak to adjacent discrete frequency bin $k-1$ and k. The FJ_CAVGPR increases robustness by collecting the signal energy leaked to adjacent frequency bins.

When k_0^* is closer to $k-1$, $\Delta = k_0^* - (k-1)$, $\Delta \in [0,\ 0.5)$, as shown in Figure 1b. When k_0^* is closer to k, $\Delta = k_0^* - k$, $\Delta \in [-0.5,\ 0)$. For the case $\Delta \in [0,\ 0.5)$, the DFT of observation at frequency bin $k-1$ and k can be expressed as follows:

$$\begin{aligned} X_l(k-1) &= A\frac{\sin(\pi\Delta)}{\sin(\pi\Delta/N)}\exp(j\varphi)\exp\left(j\pi\Delta\tfrac{N-1}{N}\right) \\ &\times \exp\left(j\tfrac{2\pi Mk_0^*}{N}l\right) + \sum_{n=0}^{N-1} g_l(n)\exp\left(-j2\pi\tfrac{k-1}{N}n\right), \end{aligned} \tag{17}$$

$$\begin{aligned} X_l(k) &= A\frac{\sin[\pi(\Delta-1)]}{\sin[\pi(\Delta-1)/N]}\exp(j\varphi)\exp\left[j\pi(\Delta-1)\tfrac{N-1}{N}\right] \\ &\times \exp\left(j\tfrac{2\pi Mk_0^*}{N}l\right) + \sum_{n=0}^{N-1} g_l(n)\exp\left(-j2\pi\tfrac{k}{N}n\right). \end{aligned} \tag{18}$$

For the case $\Delta \in [-0.5,\ 0)$, the DFT of observation at frequency bin $k-1$ and k can be expressed as follows:

$$\begin{aligned} X_l(k-1) &= A\frac{\sin[\pi(\Delta+1)]}{\sin[\pi(\Delta+1)/N]}\exp(j\varphi)\exp\left[j\pi(\Delta+1)\tfrac{N-1}{N}\right] \\ &\times \exp\left(j\tfrac{2\pi Mk_0^*}{N}l\right) + \sum_{n=0}^{N-1} g_l(n)\exp\left(-j2\pi\tfrac{k-1}{N}n\right), \end{aligned} \tag{19}$$

$$\begin{aligned} X_l(k) &= A\frac{\sin(\pi\Delta)}{\sin(\pi\Delta/N)}\exp(j\varphi)\exp\left(j\pi\Delta\tfrac{N-1}{N}\right) \\ &\times \exp\left(j\tfrac{2\pi Mk_0^*}{N}l\right) + \sum_{n=0}^{N-1} g_l(n)\exp\left(-j2\pi\tfrac{k}{N}n\right). \end{aligned} \tag{20}$$

In the cases of both Equations (17), (18) and (19), (20), the phase differences of sequences $X_l(k-1)$ and $X_l(k)$ are both $\exp\left(j\frac{2\pi Mk_0^*}{N}l\right)$. Therefore, $\delta(k)$ can be used to compensate for the phase difference in $X_l(k-1)$ and $X_l(k)$ simultaneously to obtain a coherent sequence $Z_l(k-1)$ and $Z_l(k)$, as follows:

$$\begin{aligned} Z_l(k-1) &= X_l(k-1)\exp[-j2\pi\delta(k)l], \\ Z_l(k) &= X_l(k)\exp[-j2\pi\delta(k)l]. \end{aligned} \tag{21}$$

Then, the expression of FJ_CAVGPR can be written by combining $Z_l(k-1)$ and $Z_l(k)$ as follows:

$$T_{FJ\_CAVGPR}(k) = \frac{1}{L}\left[\left|\sum_{l=0}^{L-1} Z_l(k-1)\right|^2 + \left|\sum_{l=0}^{L-1} Z_l(k)\right|^2\right]. \tag{22}$$

Note that $Z_l(-1) = 0$. The schematic of the FJ_CAVGPR is detailed in Figure 2.

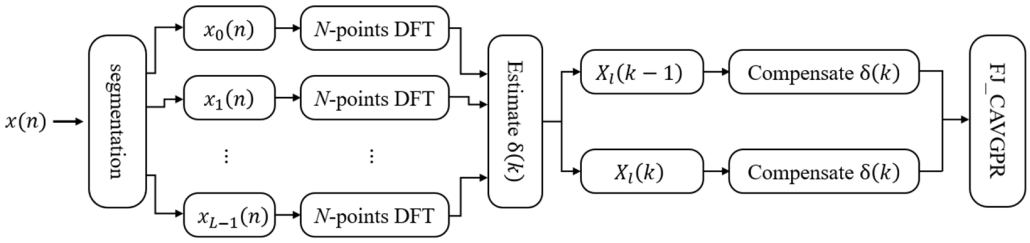

Figure 2. Schematic of the FJ_CAVGPR.

4. Simulations

In this section, the detection performance of the proposed FJ_CAVGPR is compared with those of the AVGPR, CGLRT and CAPSE via simulation.

The detection results of four tonal signals buried in WGN are presented in Figure 3. The segment number is $L = 32$, the length of each segment is $N = 500$ and $M = N$, which means there is no overlapping between segments. The sampling rate is $f_s = 1000$ Hz,

the frequencies of the four tones are 100.5 Hz, 200 Hz, 301 Hz and 399.5 Hz, respectively corresponding to $\Delta = 0.25$, $\Delta = 0$, $\Delta = -0.5$ and $\Delta = -0.25$. The SNR of each frequency is -25 dB. In this study, the SNR is defined as follows:

$$SNR = 10\lg\left(\frac{A^2}{2\sigma_g^2}\right). \tag{23}$$

As can be seen in Figure 3a the AVGPR fails to distinguish the first tone, and contains several false alarms. The CGLRT and CAPSE in Figure 3b,c have poor detection performance on the tone with $\Delta = -0.5$. Meanwhile, the FJ_CAVGPR can successfully detect the tonal signals, as shown in Figure 3d. It is noticed that the detected frequencies in Figure 3b,c are at 100 Hz, 200 Hz, 300 Hz, and 400 Hz. However, those in Figure 3d are at 102 Hz, 200 Hz, 302 Hz, and 400 Hz. This is because more energy enters the next frequency bin due to the presence of noise. In fact, the amplitude at 100 Hz and 300 Hz in Figure 3d is also obviously high, which makes the peak wider and easier to detect.

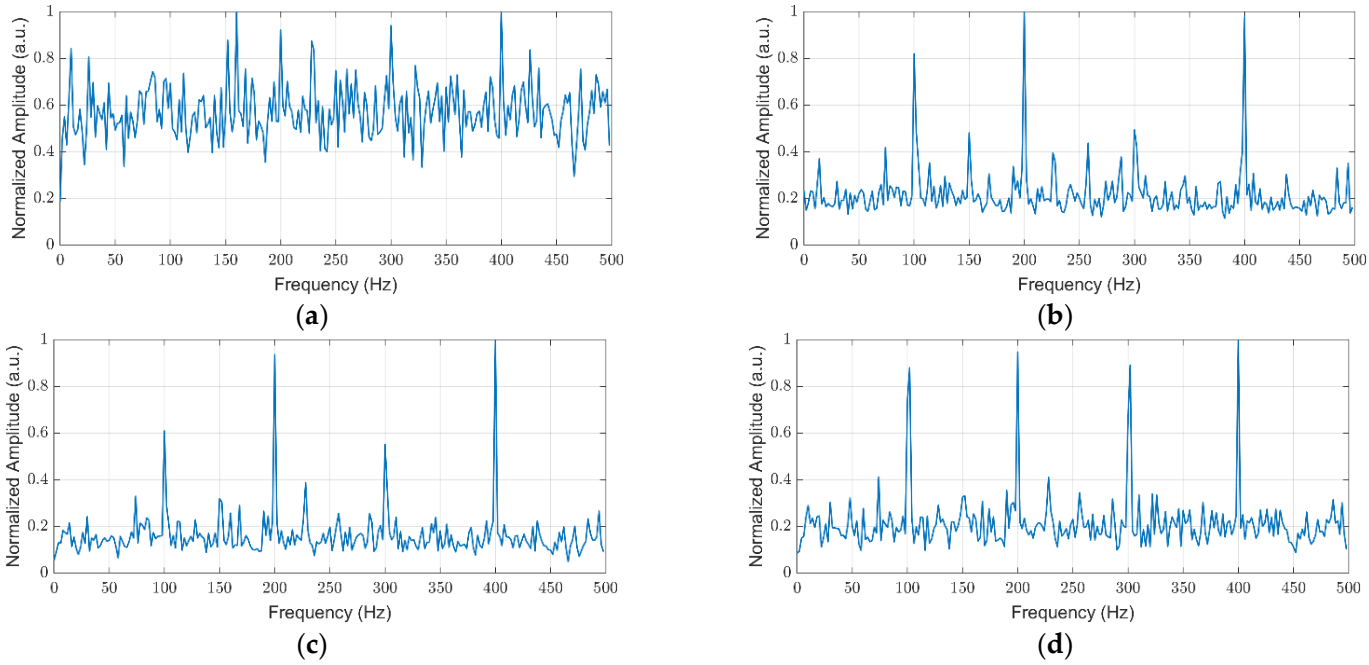

Figure 3. Detecting the four tonal signals in WGN: (**a**) AVGPR; (**b**) CGLRT; (**c**) CAPSE; (**d**) FJ_CAVGPR.

Next, the probability of detection (P_D) versus SNR curves that indicates the minimal input SNR required to reach the given P_D for a fixed probability of false alarm (P_{FA}) is used to evaluate the detection performance of the four detectors. P_D versus SNR curves for $|\Delta| = 0$ and $|\Delta| = 0.5$ at $P_{FA} = 10^{-2}$ is obtained from 10,000 Monte Carlo trials, as shown in Figure 4. The noise is additive WGN, the sampling rate is $f_s = 1000$ Hz, $L = 32$, $N = 500$, and $M = N$. As can be seen that from $|\Delta| = 0$ to $|\Delta| = 0.5$, the required SNR of AVGPR, CGLRT and CAPSE to achieve a given P_D (e.g., $P_D = 0.9$) is increased by about 3.9 dB. And FJ_CAVGPR only improves by about 1.5 dB. In other words, FJ_CAVGPR has a processing gain of 2.4 dB in this circumstance. On the other hand, it is found that when $|\Delta| = 0$, the FJ_CAVGPR is 0.5 dB worse than CAPSE. Because in this case, the signal in the adjacent frequency bin is noise rather than useful information. It appears as higher background noise in the time-frequency diagram or spectrum diagram as shown in Figure 3c,d. Nevertheless, in practice, we found that this 0.5 dB loss had little impact to the result. Therefore, it is believed that this loss is worthwhile compared with the processing gain in practical applications, the proposed FJ_CAVGPR shows good robustness against PFE.

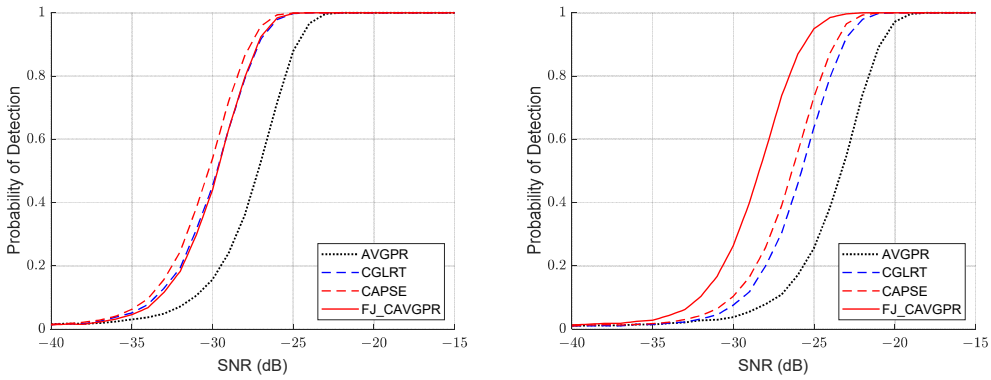

Figure 4. Detection performance of the four detectors at $P_{FA} = 10^{-2}$: (**a**) $|\Delta| = 0$; (**b**) $|\Delta| = 0.5$.

5. Experiment

A sea experiment was conducted 45 km south of Sanya, Hainan Province, in January 2019. The water depth of the experimental area was 90 m, the sound speed in the water body was basically the same, about 1532 m/s, and the sea state was level II. In the experiment, an acoustic transducer was transported by an unanchored boat, and transmitted wideband noise containing 3.5 kHz and 4 kHz tonal signals. The acoustic signal was received by a hydrophone, which was at a depth of 40 m and a distance of about 3 km from the transducer. The sampling frequency of receiving system was 10 kHz. The hydrophone used in the experiment was customized, with a received voltage response of -171 dB $\pm$ 1 dB re 1 V/µPa from 2 kHz to 5 kHz. In order to compare the methods under low SNR condition, we added tonal signals of 2 kHz, 2.5 kHz, 3 kHz. Among them, the tone of 2.5 kHz and 4 kHz were stronger, and the others were relatively weak.

The Low-Frequency Analysis and Recording (LOFAR) is used to evaluate the performance of the proposed and reference methods. The LOFAR gram can be regarded as the time-frequency diagram of time on the vertical axis, and the tonal signal appears in the form of line spectrum in the diagram. The results can be intuitively compared from the LOFAR gram. The more obvious and continuous the spectral lines, the better the processing performance. Then, by taking a segment number of $L = 16$, $N = 2048$, $M = 1024$ with 50% overlapping, the processing results are shown in Figure 5. For a more intuitive comparison, we show the amplitude and test statistics rather than the binary test results, where the amplitude of AVGPR, CAPSE, and FJ_CAVGPR are normalized and expressed in dB.

As can be seen in Figure 5a, the AVGPR cannot detect the tone of 2 kHz, while the tone of 3.5 kHz is difficult to distinguish due to the strong interference nearby. The CGLRT and CAPSE respectively shown in Figure 5b,c are superior to AVGPR, but the tones at 2 kHz, 3 kHz and 3.5 kHz cannot be detected continuously. In contrast, the above tones can be distinguished more clearly and continuously by FJ_CAVGPR, as shown in Figure 5d. This is because the proposed method utilizes the energy of adjacent frequency points to generate wider and brighter spectral lines on the graph. Therefore, the detector proposed in this study is also considered to be more reliable with real data when compared with the other examined methods.

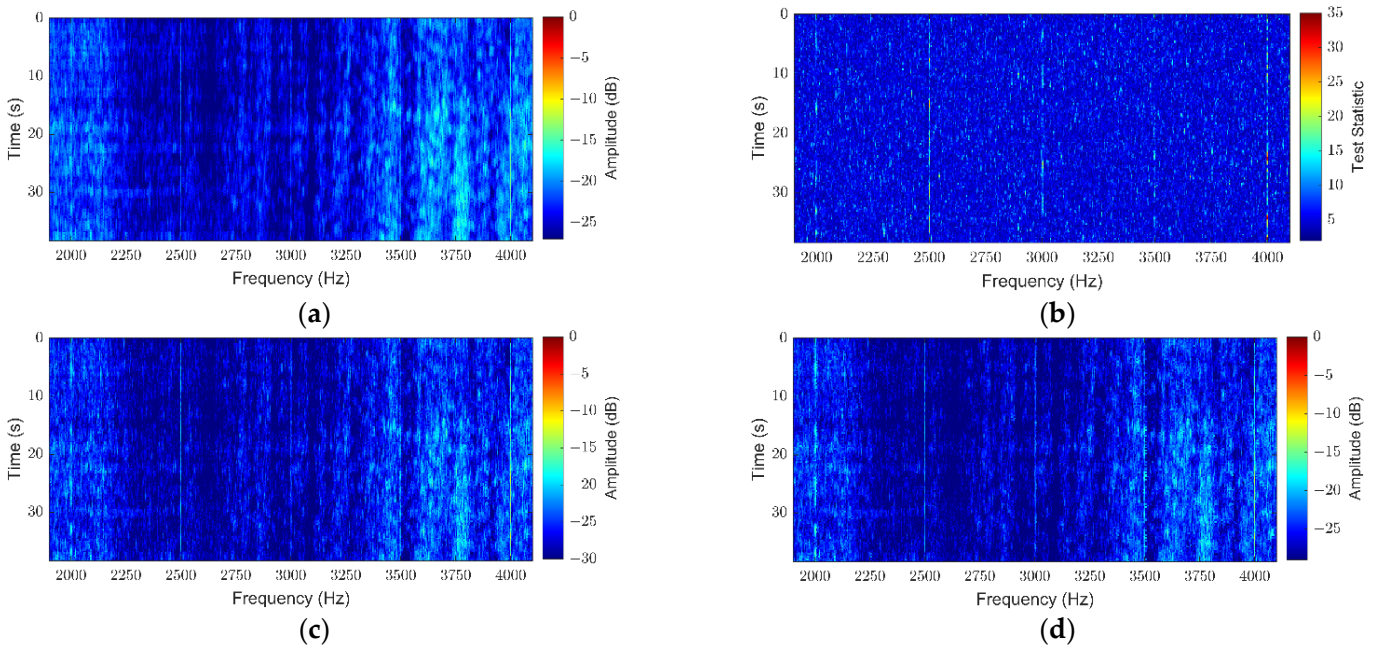

Figure 5. Experimental LOFAR of: (**a**) AVGPR; (**b**) CGLRT; (**c**) CAPSE and (**d**) FJ_CAVGPR.

6. Conclusions

PFE or scalloping loss will degrade the performance of DFT-based tonal detectors. In this study, we focus on the robust detection of tonal signals in the presence of PFE, and propose an improved coherently-average power processor. The proposed detector coherently utilizes the information from adjacent discrete frequency bins to collect the energy that leaked into them. Both the simulation and experimental results reveal that the proposed detector achieves better robustness against PFE and more reliable with real data when compared with the AVGPR, CGLRT and CAPSE. When PFE exists, the proposed method has a processing gain of 2.4 dB compared with other methods.

In future, the sparsity of the tonal signal in frequency domain should be used, and the adaptive phase compensation method could be developed.

Author Contributions: Conceptualization, C.C., Y.L. and H.H.; methodology, Q.X.; software, S.J.; formal analysis, G.W.; resources, Y.L. and H.H.; data curation, S.J.; writing—original draft preparation, Q.X.; writing—review and editing, C.C. and G.W.; funding acquisition, C.C. and S.J. All authors have read and agreed to the published version of the manuscript.

Funding: This research was funded by The National Natural Science Foundation of China, grant number 62001469 and 62201565.

Institutional Review Board Statement: Not applicable.

Informed Consent Statement: Not applicable.

Data Availability Statement: Data sharing not applicable.

Conflicts of Interest: The authors declare no conflict of interest.

References

1. Urick, R.J. *Principles of Underwater Sound*, 3rd ed.; Peninsula Publising: Los Atlos, CA, USA, 1983.
2. Whalen, A.D. *Detection of Signals in Noise*; Academic Press: Cambridge, MA, USA, 2013.
3. Arthur, B.; Walter, M. The Heard Island feasibility test. *Phys. Today* **1992**, *45*, 22–30.
4. Kay, S.M. *Fundamentals of Statistical Signal Processing. Detection Theory*; Prentice Hall PTR: Hoboken, NJ, USA, 1998; Volume 2, pp. 1545–5971.
5. Wan, C.R.; Goh, J.T.; Chee, H.T. Optimal tonal detectors based on the power spectrum. *IEEE J. Ocean. Eng.* **2000**, *25*, 540–552.
6. Welch, P. The use of fast Fourier transform for the estimation of power spectra: A method based on time averaging over short, modified periodograms. *IEEE Trans. Audio Electroacoust.* **1967**, *15*, 70–73. [CrossRef]

7. Wagstaff, R.A. The AWSUM filter: A 20-dB gain fluctuation-based processor. *IEEE J. Ocean. Eng.* **1997**, *22*, 110–118. [CrossRef]
8. Kay, S.M.; Gabriel, J.R. Optimal invariant detection of a sinusoid with unknown parameters. *IEEE Trans. Signal Process.* **2002**, *50*, 27–40. [CrossRef]
9. Qing, W.; Wan, C.; Goh, J.T. Theoretical performance analysis and simulation of a GLRT tonal detector. In Proceedings of the MTS/IEEE Oceans 2001, An Ocean Odyssey. (IEEE Cat. No. 01CH37295), Honolulu, HI, USA, 5–8 November 2001; Volume 3.
10. Scharf, L.L.; Friedlander, B. Matched subspace detectors. *IEEE Trans. Signal Process.* **1994**, *42*, 2146–2157. [CrossRef]
11. Wang, Q.; Wan, C.R. A novel CFAR tonal detector using phase compensation. *IEEE J. Ocean. Eng.* **2005**, *30*, 900–911. [CrossRef]
12. Lan, H.; White, P.R.; Li, N.; Li, J.; Sun, D. Coherently averaged power spectral estimate for signal detection. *Signal Process.* **2020**, *169*, 107414. [CrossRef]
13. Zhu, C.; Gaggero, T.; Makris, N.C.; Ratilal, P. Underwater Sound Characteristics of a Ship with Controllable Pitch Propeller. *J. Mar. Sci. Eng.* **2022**, *10*, 328. [CrossRef]
14. Vashishtha, G.; Kumar, R. Autocorrelation energy and aquila optimizer for MED filtering of sound signal to detect bearing defect in Francis turbine. *Meas. Sci. Technol.* **2021**, *33*, 015006. [CrossRef]
15. Oppenheim, A.V. *Discrete-Time Signal Processing*; Pearson Education India: Delhi, India, 1999.
16. Gandhi, C.P.; Xiang, J.; Kumar, A.; Vashishtha, G.; Kant, R. Maximal overlap discrete wavelet packet transforms-based bipolar neutrosophic cross entropy measure for identification of rotor defects. *Measurement* **2022**, *200*, 111577. [CrossRef]
17. Vashishtha, G.; Chauhan, S.; Yadav, N.; Kumar, A.; Kumar, R. A two-level adaptive chirp mode decomposition and tangent entropy in estimation of single-valued neutrosophic cross-entropy for detecting impeller defects in centrifugal pump. *Appl. Acoust.* **2022**, *197*, 108905. [CrossRef]
18. Brooker, A.; Humphrey, V. Measurement of radiated underwater noise from a small research vessel in shallow water. *Ocean. Eng.* **2016**, *120*, 182–189. [CrossRef]
19. Li, Y.F.; Chen, K.F. Eliminating the picket fence effect of the fast Fourier transform. *Comput. Phys. Commun.* **2008**, *178*, 486–491. [CrossRef]
20. Chen, S. Improving coherent tonal detection with phase interpolation and compensation. In Proceedings of the 2013 OCEANS-San Diego, San Diego, CA, USA, 23–27 September 2013.